Available online at www.sciencedirect.com
SCIENCE DIRECT®
Catalysis Today 90 (2004) 199–206
CATALYSIS TODAY
www.elsevier.com/locate/cattod

The NO selective reduction on the $La_{1-x}Sr_xMnO_3$ catalysts

Xiaodong Wu*, Luhua Xu, Duan Weng

Department of Materials Science & Engineering, Tsinghua University, Beijing 100084, China

Abstract

$La_{1-x}Sr_xMnO_3$ ($x = 0$, 0.1, 0.3, 0.5, 0.7) perovskite-type oxides (PTOs) were prepared by coprecipitation under various calcination temperature, and their performances for the NO reduction were evaluated under a simulated exhaust gas mixture. The X-ray diffraction (XRD) and thermogravimetric analysis were carried out to find the formation process of the perovskite. The NO reduction rate under different reaction temperature, the concentration of oxygen and the presence of hydrocarbon were observed by the input/output analysis. In the presence of 10% excess oxygen, the catalyst $La_{0.7}Sr_{0.3}MnO_3$ calcined at 900 °C showed a NO reduction rate of 61% at 380 °C. The study of the reaction curves showed that C_3H_8 could act as the reducer for the NO reduction below 400 °C. The NO reduction is highly affected by increasing the O_2 concentration from 0.5 to 10%, especially at high temperatures when oxygen becomes more competitive than NO on the oxidation of C_3H_8, leading to a decrease of the NO reduction from 100% to zero at 560 °C.

Keywords: Perovskite; Coprecipitation; Nitrogen oxides; Lean exhaust

1. Introduction

In the recent 20 years, perovskite-type oxides (PTOs) have been recognized as active catalysts for a variety of reactions, especially in environmental catalysis such as the catalytic combustion of hydrocarbons, decomposition of volatile organic compounds (VOCs) and auto-exhaust treatment [1–3]. Recently, under the more stringent requirement of diesel engine exhaust control, many studies have been conducted on selective reduction catalysts and noble metals and PTOs are found to be active for NO_x reduction with hydrocarbons under lean condition. For the $LaMnO_3$ perovskite, if the La^{3+} and Mn^{3+} ions are partially substituted by Sr^{2+}, Ba^{2+}, Ce^{4+}, etc. and Cu^{2+}, Zn^{2+}, Co^{3+}, etc., respectively, the perovskite lattice is distorted and structural defections are formed, resulting in an enhancement in lattice oxygen mobility and the catalytic properties of active B cation. Therefore, PTOs are potential alternatives as effective catalyst for NO_x reductions [2,4–6].

For the reactions in the auto-exhausts, the perovkite catalysts are very sensitive with the gas composition. For example, the NO reduction curves show different patterns in lean condition (such as diesel engine exhaust) and stoichiometric condition (such as gasoline engine exhaust). Normally in lean condition, NO reduction reaches a peak value in a certain temperature, and then decreases in elevated temperature. In stoichimetric condition, the NO reduction rate increases with increment of the reaction temperature. A 100% reduction rate can be achieved at about 400 °C or lower. Such a difference may be explained by the different catalysts used in different reaction systems [7–9]. But even for a same catalyst, different exhaust patterns also crucially affect the NO reduction procedure. In the lean exhaust, the oxygen concentration is normally 10% or even higher, no CO presents, and the evaporated hydrocarbon concentration is only 200×10^{-6}. While in stoichimetric condition, the exhaust contains about 1.5% oxygen, 1% CO and 500×10^{-6} hydrocarbon [10].

In this paper, the catalytic performance of $La_{1-x}Sr_xMnO_3$ for the NO reduction was studied. The NO reduction behavior of these PTOs with varied calcination temperatures and varied amounts of strontium (Sr) substitution were observed and the active component was recognized. The effects of the reaction temperature, the oxygen concentration and the presence of hydrocarbon on the catalytic activity were discussed.

* Corresponding author. Tel.: +86-10-62792375; fax: +86-10-62772726.
E-mail address: wuxiaodong@tsinghua.edu.cn (X. Wu).

0920-5861/$ – see front matter © 2004 Elsevier B.V. All rights reserved.
doi:10.1016/j.cattod.2004.04.027

2. Experimental

2.1. Preparation of catalysts

To prepare $La_{1-x}Sr_xMnO_3$, the $La(NO_3)_3$, $Sr(NO_3)_2$, $Mn(NO_3)_2$ solutes were mixed according to the molar ratio of La:Sr:Mn = 1–*x*:*x*:1(x = 0, 0.1, 0.3, 0.5, 0.7, from the sample 1# to 5# in turn). NaOH (2 mol/l) and Na_2CO_3 (1 mol/l) were mixed by equal volume as precipitator. Then the solution and the precipitator were mixed together, filtrated and washed to obtain the precursor powders (deposited carbonate and hydrate of La, Sr, Mn). The precursor was calcined at different temperature from 600, 750 to 900 °C for 3 h. The particle size of the resulting powder catalyst was ranged from dozens of nanometer to hundreds of nanometer. Each sample was weighed out 1.5 g and then was mixed homogeneously with 6 ml quartz particles (chemically stable and low absorption pattern) to be used for activity evaluation.

2.2. Catalytic activity studies

The catalyst mixture was loaded in a quartz reaction tube with the diameter of 25 mm. The catalytic activity was evaluated in a tube micro-reactor by passing a simulated exhaust gas mixture. The simulated exhaust contained a mixture of O_2 (10%, 3% or 0.5%), NO (500×10^{-6}), C_3H_8 (200×10^{-6}), SO_2 (50×10^{-6}), CO_2 (8%), H_2O (6%) and N_2 (balance). For the light-off experiments, the reactor was heated from 100 to 600 °C in the flow stream at a gas space velocity of 35,000 h^{-1}. The concentrations of NO and C_3H_8 were recorded on-line. It should be noted that here the NO concentration determined by the Shimadzu NOA-7000 NO_x analyzer stands for the total nitrogen oxides (NO plus a little NO_2 and other NO_x), this is more reasonable to reveal the NO reduction (to N_2 and O_2).

2.3. Characterization of catalysts

The X-ray diffraction (XRD) analysis was conducted on a Japan Science D/max-RB diffractometer employing Cu Kα radiation (λ = 1.5418 Å, DS = 1°). The X-ray tube was operated at 45 kV and 150 mA. The X-ray powder diffractograms were recorded at 0.02° intervals in the range $20° \leq 2\theta \leq 80°$ with 2 s count accumulation per step. The thermal decomposition with the temperature increment was performed in air by using a SETARAM TGA-92 thermogravimetric analyzer. The powder samples (ca. 0.3 g) were heated from 60 up to 900 °C at the rate of 10 °C/min during TGA measurements. The specific surface area was determined by Brunauer–Emmett–Teller (BET) method with a Quan-

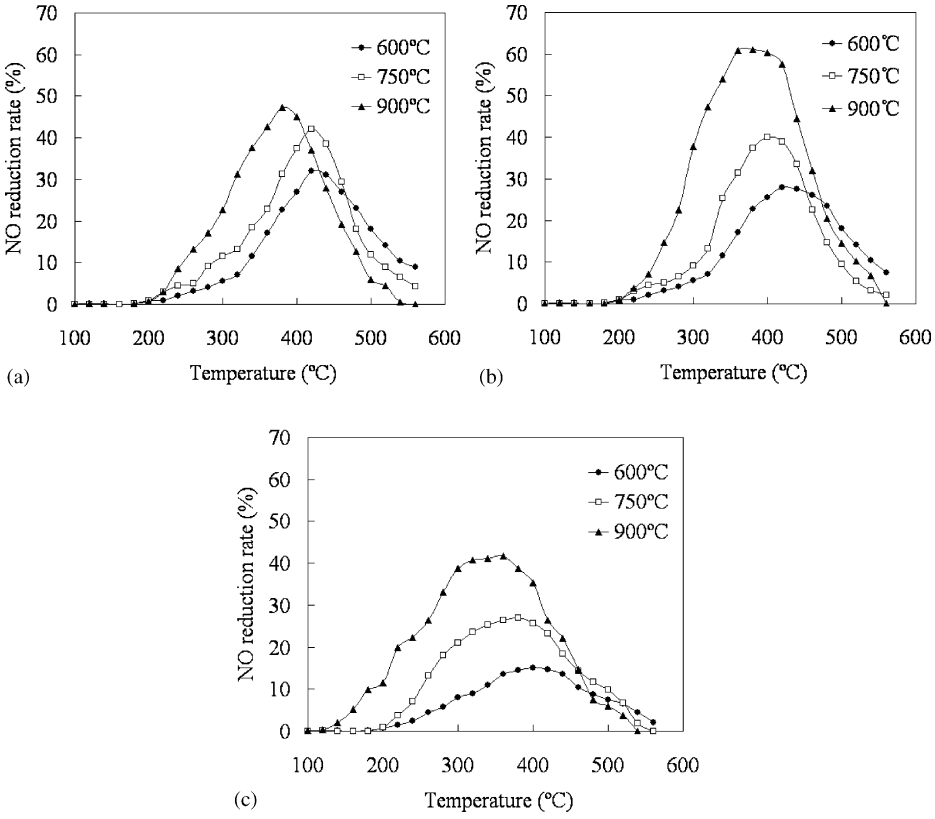

Fig. 1. NO reduction curves of the samples with different calcination temperature: (a) $La_{0.9}Sr_{0.1}MnO_3$ (2#); (b) $La_{0.7}Sr_{0.3}MnO_3$ (3#); (c) $La_{0.5}Sr_{0.5}MnO_3$ (4#).

tachrome NOVA instrument using Ar as carrier and N_2 as adsorbent.

3. Results and discussion

3.1. Effect of calcination temperature on catalytic activity

The precursor particles of $La_{1-x}Sr_xMnO_3$ were calcined at 600, 750, and 900 °C for 3 h, respectively. The effect of varied calcination temperature on the catalytic activity was investigated, and the NO reduction curves for 2#, 3#, and 4# ($x = 0.1, 0.3, 0.5$) are shown in Fig. 1. The result shows that the higher the calcination temperature, the better the catalytic activity for the NO reduction. It can be seen from Fig. 1b that the sample 3# has a best reduction rate of 28% at 440 °C for the sample calcined at 600 °C while that for the sample calcined at 750 °C is 41% at 400 °C. When the calcination temperature is enhanced up to 900 °C, the peak value of de-NO catalytic activity evidently increases to 61% at 380 °C. The similar phenomenon occurs over the sample 2# and 4#. This suggests that different phase structure may exist in the samples calcined at different temperature.

In order to find out the active component in the samples after different calcination temperature, a thermogravimetric analyzer was used to analyze the phase transition with the temperature ranged from 60 to 900 °C. The TGA patterns of 2#, 3#, and 4# are presented in Figs. 2a, 3a and 4a, respectively. The X-ray diffraction patterns of the corresponding samples calcined at different temperature are also shown in Figs. 2b, 3b and 4b, respectively. From the TGA curves, it can be seen that a series of mass loss occurred at various temperature, which correspondingly suggests the occurrence of some chemical reactions. Combine with the XRD patterns and some decomposition parameters of these compounds, we can roughly conclude the reactions during the whole process as follows.

The TGA curve can be divided into several steps according to the change of the slope. The temperature inflexions shows a small difference from one to another, say the first one in Fig. 2a, 3a and 4a are 340, 350, and 380 °C, respectively. It is primarily due to the variations of the precursor composition and particular preparation process. However, these TGA curves are substantially similar. Take example by the sample 2# presented in Fig. 2. Some chemical equations are described in Table 1, corresponding to a certain mass loss. The first 7% mass loss between room temperature and 340 °C is the loss of physical- and chemical-adsorbed water from several kinds of hydrates. During the temperature from 340 to 460 °C, the carbonates of La^{3+} and Mn^{2+} begin to release CO_2, leading to another 12% mass loss. After that, a 7% mass loss occurs from 460 to 740 °C. It means MnO_2 begins to release O_2 gradually and the perovskite $aMnO_3$ and $La_{1-x}Sr_xMnO_3$ phase begins to form near 800 °C.

When the temperature is higher than 740 °C, the decomposition of $SrCO_3$ brings another mass loss. In the XRD patterns, the peaks of SrO gradually weaken and eventually disappear with increment of the calcination temperature. It is suggested that this mass loss is also related to the formation of Sr-doped perovskite, in which the valence of Mn may change from Mn^{3+} to Mn^{4+} and oxygen is released to form nonstoichiometric PTOs. For the sample 2#, the mass loss is not considerable from 740 to 900 °C since it contains only a little Sr in the precursor. However, it is much more obvious for the sample 3# and 4# shown in Figs. 3 and 4, respectively. The mass loss ratio of 2#, 3#, and 4# in this region is about 1:3:5, which is consistent with the amount of Sr additive in different samples. Current theory on the dynamics of the perovskite catalyst is that the defect positions induced by additives make the perovskite more active, in which the oxygen vacancies and cationic defects act as active positions. Therefore, it can be concluded that the higher the calcination temperature, the more completely

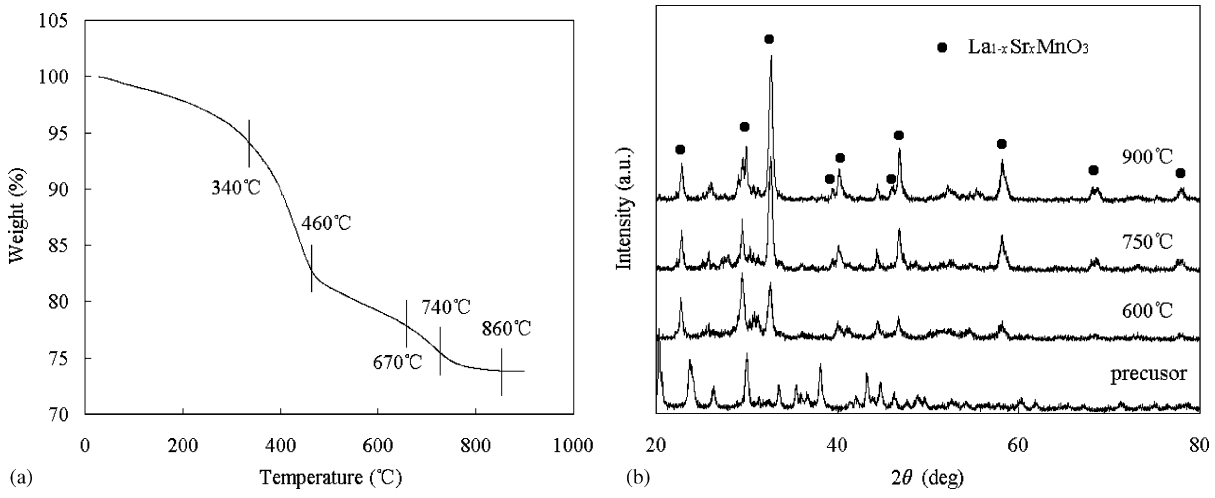

Fig. 2. (a) TGA and (b) XRD patterns of the $La_{0.9}Sr_{0.1}MnO_3$ (2#) sample.

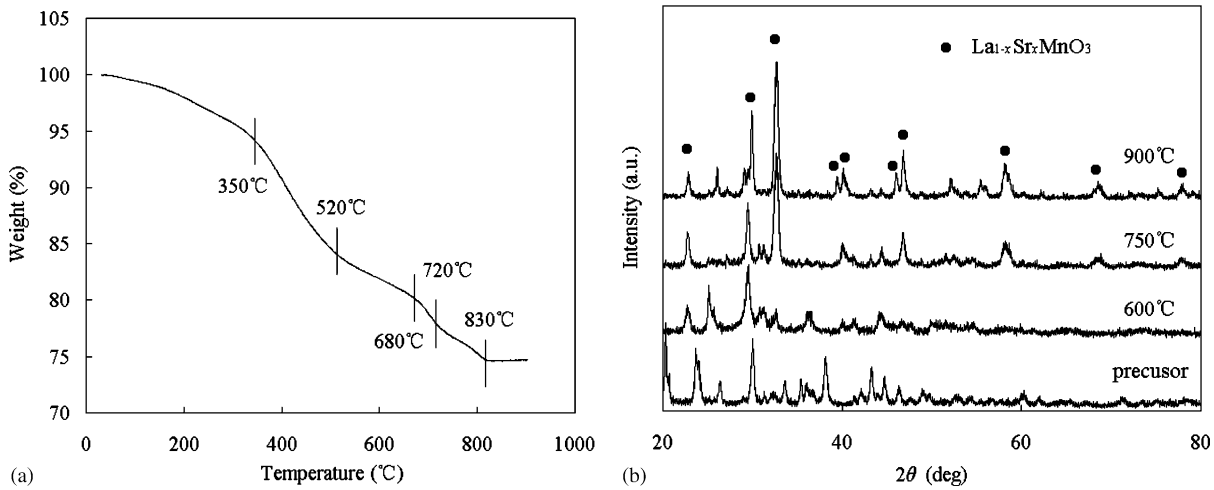

Fig. 3. (a) TGA and (b) XRD patterns of the $La_{0.7}Sr_{0.3}MnO_3$ (3#) sample.

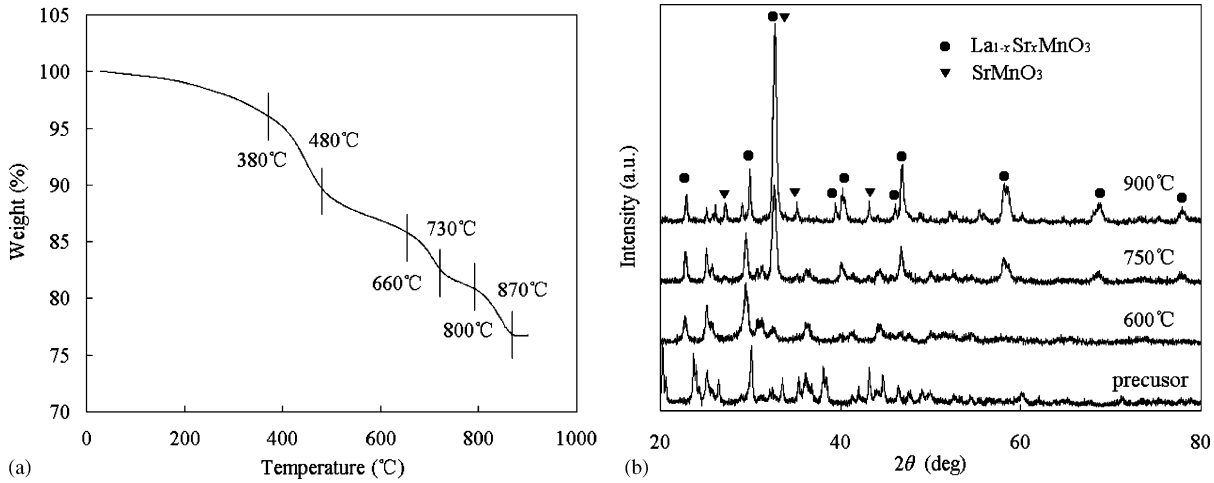

Fig. 4. (a) TGA and (b) XRD patterns of the $La_{0.5}Sr_{0.5}MnO_3$ (4#) sample.

the Sr-doped perovskite forms, and the higher the catalytic activity may be.

3.2. Effect of Sr additive on catalytic activity

It was suggested in Fig. 1 that the amount of Sr additive can affect the catalytic activity. Here, the quantitative effect of Sr additive on catalytic activity and the role of Sr are investigated. A series of $La_{1-x}Sr_xMnO_3$ samples were calcined at 900 °C. Their catalytic activities on the NO reduction and the C_3H_8 oxidation were evaluated and the results are shown in Fig. 5.

For all the five samples, it can be seen from Fig. 5a that with increment of the reaction temperature, the NO reduc-

Table 1
Chemical reactions in varied temperature region

Temperature region	Reactions may occur
Room temperature–340 °C	$La(OH)CO_3 \rightarrow La_2O_3 + La_2(CO_3)_3 + H_2O$ $Mn(OH)_2CO_3 \rightarrow MnO_2 + Mn(CO_3)_2 + H_2O$
340–460 °C	$La_2(CO_3)_3 \rightarrow La_2O_3 + CO_2$ $Mn(CO_3)_2 \rightarrow MnO_2 + CO_2$
460–740 °C	$La_2O_3 + MnO_2 \rightarrow LaMnO_3 + O_2$, $La_2O_3 + MnO_2 + SrCO_3 \rightarrow La_{1-x}Sr_xMnO_3 + O_2 + CO_2$(~740 °C)
740–860 °C	$SrCO_3 \rightarrow SrO + CO_2$ $La_{1-x}Sr_xMnO_3 + SrO \rightarrow La_{1-y}Sr_yMnO_3$ $La_{1-y}Sr_yMnO_3 \rightarrow La_{1-y}Sr_yMnO_{3-z} + O_2$

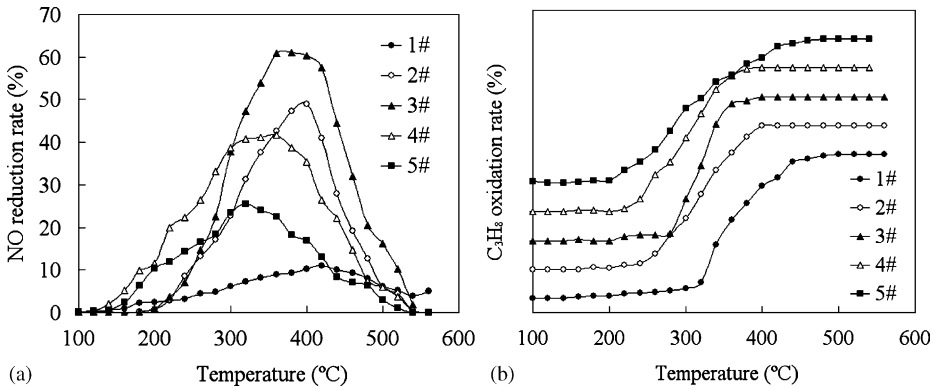

Fig. 5. (a) NO reduction and (b) C_3H_8 oxidation curves of the $La_{1-x}Sr_xMnO_3$ samples, where 1–5# refers to $x = 0$, 0.1, 0.3, 0.5, and 0.7, respectively.

tion rate increases firstly, reaches peak value, and then decreases to zero at elevated temperatures. In comparison with the pure $LaMnO_3$ catalyst 1#, the NO reduction rate is enhanced obviously over the sample 2# and 3# with a little Sr additive. However, while too much Sr additive is added, such as 4# and 5#, it leads to a decreased de-NO activity. The sequence of NO reduction activity over these PTOs is: 3# > 2# > 4# > 5# >1#. The peak value of NO reduction rate for the sample 1–5# is 11, 49, 61, 40, and 20%, respectively. The corresponding reaction temperature is 420, 400, 380, 360, and 320 °C, respectively. It is an interesting feature that the position of the peak value of NO reduction shifts toward lower temperatures with increment of the Sr additive. Correspondingly, the light-off characteristic for propane oxidation shows a similar pattern in Fig. 5b (20% intervals between every two curves). The light-off temperature T_{10} (HC) of the sample 5# is ca. 220 °C, which is 100 °C lower than that (ca. 320 °C) of the sample 1#. This is related to the effect of propane as the reducer for NO, which will be discussed below. On the other hand, the sequence of 100% conversion rate of propane is: 4# > 3# > 2# > 5# >1#, which is approximately consistent with that of the NO reduction activity.

The XRD results of the perovskite catalysts with different Sr additive ($x = 0.1$, 0.3, 0.5, 0.7) calcined at 900 °C are shown in Fig. 6. It can be seen that the phase composition changes with various amount of Sr introduced into the complex oxides. For the sample 2# and 3#, a small amount of Sr additive can ultimately enter into the perovskite lattice and form $La_{1-x}Sr_xMnO_3$ phase. When more Sr is added, the excess Sr cations react with MnO_2 and form $SrMnO_3$, which is considerable in the sample 4# and 5#. According to the conversion curves in Fig. 5, it seems that the $SrMnO_3$ does not contribute to the NO reduction.

The BET surface areas of the samples calcined at 900 °C were also measured and the result is presented in Table 2. Their BET surface areas range from 12 to 29 m^2/g with most of the samples at 20 ± 3 m^2/g. It seems that the surface area increases with increment of the Sr additive. However, the BET surface area of the sample 5# unexpectedly decreases. Furthermore, the sample 4# with largest surface area is not provided with the best NO reduction activity. Hereby, no

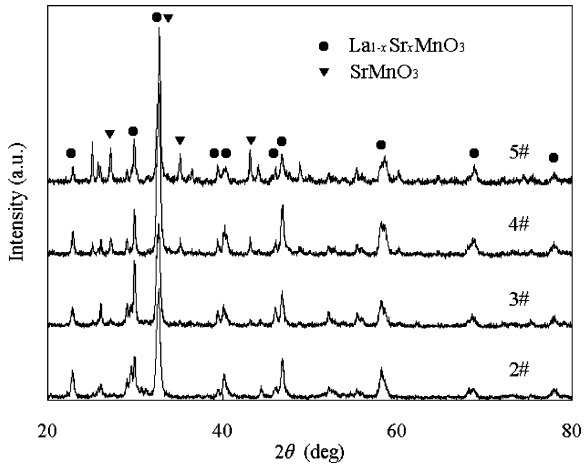

Fig. 6. X-ray diffraction patterns of the $La_{1-x}Sr_xMnO_3$ samples, where 2–5# refers to $x = 0.1$, 0.3, 0.5 and 0.7, respectively.

direct trends are observed associated with composition and catalytic performance of these PTOs, and the differences in BET areas primarily reflect differences in synthesis methods.

From what discussed above, it becomes clear that the main active component in the samples is the Sr-doped $La_{1-x}Sr_xMnO_3$ perovskite. When about 30% Sr additive was introduced to replace La^{3+} cation and the precursor was calcined at a temperature of 900 °C, the resulting powder catalyst processes a best catalytic activity for NO reduction. Why the catalytic activity is influenced by the amount of Sr additive can be explained by the theory of oxygen vacancies and cationic defects [11–13]. Since Sr^{2+} is bivalent ion and La^{3+} is trivalent ion, other ions such

Table 2
BET surface areas of $La_{1-x}Sr_xMnO_3$ at 900 °C

No.	Nominal composition	BET surface area (m^2/g)
1#	$LaMnO_3$	12
2#	$La_{0.9}Sr_{0.1}MnO_3$	19
3#	$La_{0.7}Sr_{0.3}MnO_3$	23
4#	$La_{0.5}Sr_{0.5}MnO_3$	29
5#	$La_{0.3}Sr_{0.7}MnO_3$	17

as O^{2-} will change their status to meet the electrovalence balance when Sr enters into the $LaMnO_3$ perovskite lattice to form an $(AA')BO_3$ phase. With a few Sr^{2+} cations take up the A-site, the adjacent O^{2-} anions on the dodecahedron sites become more active. It tends to deviate from the lattice, leaving a vacancy in this site. If the oxygen vacancy is located on the surface of the catalyst, some gas molecules such as NO will be adsorbed and activated, attributed to a high NO reduction rate.

3.3. Relationship of O_2, C_3H_8, NO during the reactions

Overall, the NO reduction procedure in the simulated lean exhaust is still uncertain and the effects of O_2 and C_3H_8 on the NO reduction are still unclear. Temperature programmed desorption (TPD) and temperature programmed reduction (TPR) may be used for surface chemical analysis to construct a model for the catalytic reaction procedure [14,15]. However, one disadvantage of these methods is that the input gas must be simplified and Ar or He is normally used as the background flow. In this paper, an input/output analysis was applied to study the relationship between O_2, C_3H_8, and NO in the catalytic reactions over PTOs. The mass flow meters were used to adjust the content of the input simulated exhaust, especially the oxygen concentration, and then the effect on the reactions can be revealed. Although this method can not give the details about the reaction procedure, it is useful to analyze the catalytic mechanism of the samples under various air/fuel conditions.

To find out why a peak point exists in the NO reduction curve, the relationship between the reactions of NO and C_3H_8 are firstly investigated. By putting the conversion curves of NO and C_3H_8 together in one figure, it can be seen from Fig. 7 that the onsets of the NO reduction and the C_3H_8 oxidation start almost simultaneously. And then they increase together with increment of the reaction temperature. When C_3H_8 is ultimately fully oxidized, the NO reduction curve reaches its peak point. Then C_3H_8 keeps a full conversion rate while the NO reduction rate begins to decrease to zero, which suggests that oxygen consumes most of C_3H_8 at high temperatures. Thus, it can be concluded that C_3H_8 is probably used as an oxidant for the reduction of NO at low temperatures (below 400 °C here). At high temperatures, oxygen becomes more competitive than NO on the oxidation of C_3H_8. As a result, the reduction rate of NO decreases.

By changing the oxygen concentration from 0.5 to 3% then to10% while keeping the concentrations of NO and C_3H_8 fixed in the input gas mixture, the effect of the O_2 concentration variation on the NO reduction is presented in Fig. 8. The sample 3# calcined at 900 °C is used here as the powder catalyst. When the reaction temperature is lower

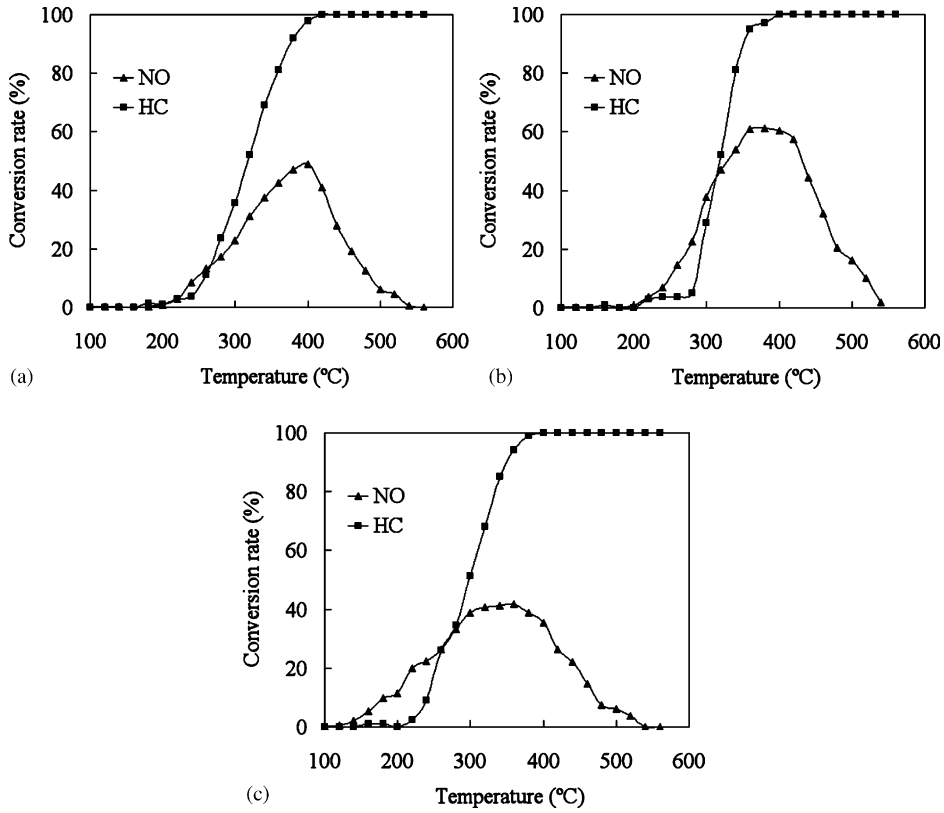

Fig. 7. Relationship between the conversion of NO and C_3H_8 over the (a) $La_{0.9}Sr_{0.1}MnO_3$ (2#), (b) $La_{0.7}Sr_{0.3}MnO_3$ (3#) and (c) $La_{0.5}Sr_{0.5}MnO_3$ (4#) samples, respectively.

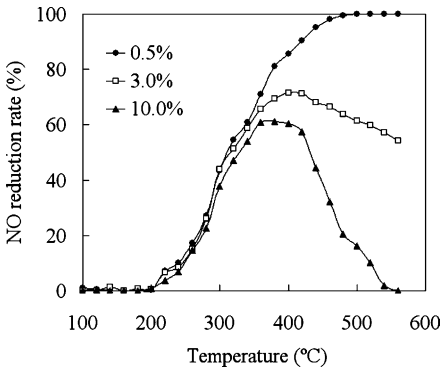

Fig. 8. NO reduction curves under various O_2 concentrations over the $La_{0.7}Sr_{0.3}MnO_3$ (3#) sample.

than 360 °C, the NO reduction rates are almost the same under these three varied oxygen concentration. However, the NO reduction curve has quite different patterns at high temperatures above 360 °C. When only 0.5% O_2 presents in the simulated exhaust, the NO reduction rate increases with increment of the reaction temperature and approaches 100% above 480 °C. On the other hand, when more O_2 like 3 and 10% exists, the NO reduction rate decreases after a peak value. The downtrend of the NO reduction curve in the case of 10% O_2 is steeper than that in the case of 3% O_2. When the reduction of NO is fully halted at 560 °C under 10% O_2, the NO reduction rate still remains 54% under 3% O_2.

In order to explore the relationship of O_2, C_3H_8, and NO reaction further, by using the oxygen concentration as the *X*-axis, the competitive activity of NO and O_2 to the oxidation of C_3H_8 is presented in Fig. 9. At the temperature of 300 °C, NO is partially reduced in the presence of C_3H_8 and the concentration of O_2 does not affect the NO reduction. Thus, NO is more active than O_2 for the C_3H_8 oxidation at this temperature. At 400 °C, the NO reduction rate increases under all three O_2 concentrations in comparison with the case at 300 °C, but the O_2 concentration begins to affect the NO–C_3H_8 reaction, which implies the O_2–C_3H_8 reaction occurs. In the case at 500 °C, especially at 560 °C, this trend shows more obviously, where the NO reduction rate reaches

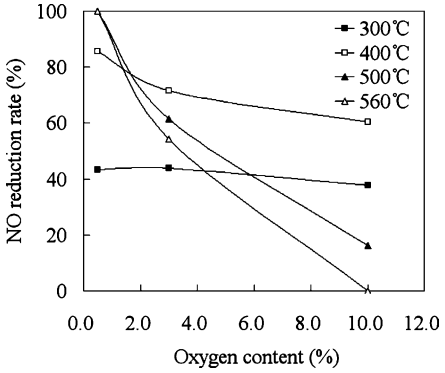

Fig. 9. Effect of the O_2 concentration variation on the NO reduction under various reaction temperatures over the $La_{0.7}Sr_{0.3}MnO_3$ (3#) sample.

100% under 0.5%O_2 and zero under 10% O_2, respectively. This indicates that the O_2–C_3H_8 reaction consumes most of C_3H_8 and the NO reduction is totally embarrassed under the presence of excess oxygen.

It can hereby be concluded that, in the catalytic reactions over the $La_{0.7}Sr_3MnO_3$ catalyst, C_3H_8 acts as a reducer for the NO reduction, and this reduction process can be prevented by oxygen, especially under higher temperature and larger oxygen concentration with most C_3H_8 consumed by O_2. It should be noted that the NO reduction procedure in the exhaust system is quite complex and affected by several factors. Different catalysts (noble metals and PTOs) have different NO reduction patterns. And with using other reducers C_2H_4, CH_4, C_3H_6 or CO for the NO reduction, the characteristic of the reaction procedure and the effect of O_2 can also be totally different [10,13,16,17].

4. Conclusions

The results show that the Sr-doped perovskite $La_{0.7}Sr_{0.3}MnO_3$ calcined at 900 °C shows a favorable NO reduction rate of 61% at 380 °C in the presence of 10% excess oxygen. Compared with the pure $LaMnO_3$ catalyst, the NO reduction rate is enhanced obviously over the samples doped with a little Sr. However, when too much Sr element is added into the complex oxides, the NO reduction rate decreases to less than 20%. By the input/output analysis, the relationship between O_2, NO, and C_3H_8 explains the different patterns of the NO reduction under different O_2 concentration. C_3H_8 can act as the reducer for NO reduction below 400 °C, but the NO reduction is severely weakened by increasing the O_2 concentration, especially at high temperatures. Oxygen becomes more competitive than NO on the oxidation of C_3H_8, leading to a decrease of the NO reduction rate. This explains why the NO reduction rate can reach 100% at 560 °C under 0.5% O_2 and become zero under 10% O_2.

Acknowledgements

The authors would like to acknowledge Project 2003AA-643010 supported by the Ministry of Science and Technology, PR China, as well as Project 50172029 supported by National Natural Science Foundation of China (NSFC). Moreover, we would also thank the Lab of Advance Materials, Tsinghua University for performing XRD, TGA and BET experiments.

References

[1] H. Tanaka, M. Misono, Curr. Opin. Solid State Mater. Sci. 5 (2001) 381.
[2] D. Fino, P. Fino, G. Saracco, S. Vito, Appl. Catal. B: Environ. 43 (2003) 243.

[3] V. Blasin-Aubé, J. Belkouch, L. Monceaux, Appl. Catal. B: Environ. 43 (2003) 175.
[4] F.C. Buciuman, E. Joubert, J.C. Menezo, J. Barbier, Appl. Catal. B: Environ. 35 (2001) 149.
[5] Y. Teraoka, K. Kanada, S. Kagawa, Appl. Catal. B: Environ. 34 (2001) 73.
[6] H. Tanaka, N. Mizuno, M. Misono, Appl. Catal. A: Gen. 244 (2003) 371.
[7] L. Borovskikh, G. Mazo, E. Kemnitz, Solid State Sci. 5 (2003) 409.
[8] C. Tofan, D. Klvana, J. Kirchnerova, Appl. Catal. A: Gen. 226 (2002) 225.
[9] R. Burch, P.J.F. Harris, C. Pipe, Appl. Catal. A: Gen. 210 (2001) 63.
[10] C. Tofan, D. Klvana, J. Kirchnerova, Appl. Catal. B: Environ. 36 (2002) 311.
[11] S.S. Hong, G.D. Lee, Catal. Today 63 (2000) 397.
[12] V.C. Belessi, T.V. Bakas, C.N. Costa, A.M. Efstathiou, P.J. Pomonis, Appl. Catal. B: Environ. 28 (2000) 13.
[13] V.C. Belessi, C.N. Costa, T.V. Bakas, T. Anastasiadou, P.J. Pomonis, A.M. Efstathiou, Catal. Today 59 (2000) 347.
[14] S. Hodjati, K. Vaezzadeh, C. Petit, V. Pitchon, Appl. Catal. B: Environ. 26 (2000) 5.
[15] C. Resini, T. Montanari, L. Nappi, G. Bagnasco, J. Catal. 214 (2003) 179.
[16] D. Ferri, L. Forni, M.A.P. Dekkers, B.E. Nieuwenhuys, Appl. Catal. B: Environ. 16 (1998) 339.
[17] T. Harada, Y. Teraoka, S. Kagawa, Appl. Surf. Sci. 121/122 (1997) 505.